

Optical Resonator Analog of a Two-Dimensional Topological Insulator

G. Q. Liang and Y. D. Chong*

*Division of Physics and Applied Physics, School of Physical and Mathematical Sciences,
Nanyang Technological University, Singapore 637371, Singapore*

A lattice of optical ring resonators can exhibit a topological insulator phase, with the direction of rotation in the resonators playing the role of spin. This occurs when the inter-resonator coupling is sufficiently large, and the synthetic magnetic vector potential set up by the couplers is zero. Using the transfer matrix method, we derive the band structure, phase diagram, and the projected band diagram showing the existence of spin-polarized edge states. When PT (parity/time-reversal) symmetric gain and loss are introduced, the system functions as an optical diode which does not require optical nonlinearities.

PACS numbers: 42.60.Da, 42.70.Qs, 73.43.-f

The idea that photonic modes could have non-trivial topological properties, analogous to topological states of quantum matter, originated some years ago with Haldane and Raghu [1, 2]. These authors argued that, in a two-dimensional (2D) photonic crystal with broken time-reversal symmetry, there should be modes analogous to the electronic modes of a “zero-field” quantum Hall gas [3]. This was soon confirmed experimentally, using a microwave-scale gyromagnetic photonic crystal [4, 5]. The most striking feature of this system is the existence of topologically-protected one-way photonic edge states, which can be used for optical isolation; unfortunately, it is difficult to scale this to optical frequencies, where magneto-optic effects are weak. Several related systems have subsequently been studied [6–11]. Of particular interest is the system proposed by Hafezi *et al.* [7], which consists of optical ring resonators arranged in a lattice, like a 2D version of the CROW (coupled resonator optical waveguide) [12]. Additional waveguides are used to couple the resonators, so that each resonator mode couples only (or mainly) to neighboring resonator modes with the same direction of rotation. In the tight-binding (weak coupling) regime, phase shifts in the inter-resonator couplings were shown to play the role of a magnetic vector potential in the tight-binding hopping amplitude, carrying opposite signs for the two directions of rotation, which play the role of spin. The couplings may be tuned so that the “magnetic field” is uniform, whereupon each spin sector exhibits Landau levels in a Hofstadter butterfly spectrum [13], with one-way edge modes which are topologically protected against spin-conserving perturbations. Although the system is reciprocal (time-reversal maps the two spin sectors onto each other), and therefore cannot be used for optical isolation, Hafezi *et al.* have suggested that its topologically-protected edge states may be used as robust optical delay lines [7].

In this Letter, we discuss some subtle and interesting features of the system of Hafezi *et al.* which do not appear in the tight-binding analysis. In the “zero field” regime,

where the synthetic magnetic vector potential induced by the inter-resonator couplings vanishes, there exists a topological insulator phase at large coupling strengths. In this phase, each spin sector exhibits an analog of the zero-field quantum Hall effect, including one-way edge states, much like the prototypical 2D topological insulator model of Kane and Mele [14]. Adding an integer number of magnetic flux quanta per unit cell maps the band structure back onto the zero field case. Our results are obtained using the transfer matrix method, which has previously been applied to the CROW [15, 16], and has a much wider domain of validity for such systems than the tight-binding method [16]. These calculations are also of interest in that they yield topological insulator physics without the use of tight-binding, or even of a Hamiltonian. Finally, as a straightforward extension of the transfer matrix analysis, we study the band structure of the PT-symmetric (parity/time-reversal symmetric [17]) lattice, which may be realized by adding equal and opposite amounts of gain and loss to parity-symmetric regions of the coupling waveguides. PT-symmetric photonic lattices are known to have several unusual properties, such as bifurcations between real and complex bands [18–21]; they have recently been realized experimentally using optical fiber networks [22], and the present system could be realizable in a similar way. We show that by adding PT-symmetric gain and loss to the couplers, we can achieve *directional* amplification, amplifying the one-way state on one edge and damping the counter-propagating state on the opposite edge.

We consider the square lattice shown in Fig. 1. At each lattice site is a ring resonator, whose modes are coupled to the modes on neighboring lattice sites having the same “spin” (direction of rotation within the resonator). As proposed in Ref. [7] and depicted in Fig. 1(c), this coupling can be implemented by using a waveguide to join the rings. However, for our present purposes it will be useful to employ a more abstract representation for the couplings. We take the spins to be completely decoupled, and restrict our attention to a single spin sector. Let $n \equiv (x_n, y_n)$ denote a lattice site, $n + \hat{x}$ denote the site one unit in the $+\hat{x}$ direction, $n + \hat{y}$ the site one unit in the $+\hat{y}$ direction, etc. We specify the coupling be-

* yidong@ntu.edu.sg

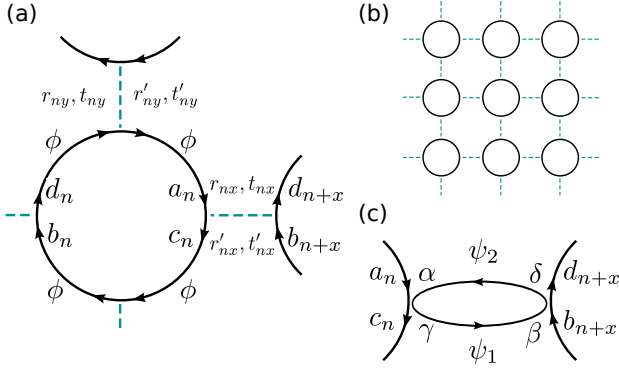


FIG. 1. Coupled optical resonators in a square lattice. (a) Schematic showing the couplings between neighboring loop resonators, including the wave amplitudes which enter into the coupling relations (1). (b) Schematic of the lattice over several periods. (c) A typical waveguide loop which can give rise to the couplings shown in (a).

tween the resonator at n and the one at $n+x$ by four complex coupling coefficients r_{nx} , r'_{nx} , t_{nx} , and t'_{nx} ; similarly, we denote the coupling between n and $n+y$ by another four coupling coefficients r_{ny} , r'_{ny} , t_{ny} , and t'_{ny} . These relate the wave amplitudes in the resonator—see Fig. 1(a)—according to

$$\begin{aligned} S_{nx} \begin{bmatrix} a_n \\ b_{n+x} \end{bmatrix} &= \begin{bmatrix} d_{n+x} \\ c_n \end{bmatrix}, \\ S_{ny} \begin{bmatrix} d_n \\ c_{n+y} \end{bmatrix} &= \begin{bmatrix} b_{n+y} \\ a_n \end{bmatrix} e^{-2i\phi}, \end{aligned} \quad (1)$$

where

$$S_{n\mu} = \begin{bmatrix} r_{n\mu} & t'_{n\mu} \\ t_{n\mu} & r'_{n\mu} \end{bmatrix}. \quad (2)$$

Here, and in the following, the dummy index μ may take the value x or y . The parameter ϕ is the phase delay across each quarter of the resonator (assumed equal). The matrices $S_{n\mu}$ have the form of scattering matrices, with $\{r_{n\mu}, r'_{n\mu}\}$ and $\{t_{n\mu}, t'_{n\mu}\}$ playing the role of “reflection” and “transmission” coefficients respectively. They express the most general possible form of linear spin-conserving coupling between the resonators. In principle, each of the coupling coefficients $\{r_{n\mu}, r'_{n\mu}, t_{n\mu}, t'_{n\mu}\}$ can be independently varied by appropriately tuning the underlying waveguide coupling parameters and phase delays [23]. In an experimental system, both ϕ and the coupling coefficients will depend implicitly on the operating frequency. However, here we will treat them as independent quantities; when calculating the bandstructure, ϕ will play the role of frequency (or energy) [16].

Now consider the special case where the “reflection” coefficients $r_{n\mu}$ and $r'_{n\mu}$ vary between different cells by some phase factor, according to

$$\begin{aligned} r_{n\mu} &= r_\mu e^{iA_n^\mu}, & r'_{n\mu} &= r'_\mu e^{-iA_n^\mu}, \\ t_{n\mu} &= t_\mu, & t'_{n\mu} &= t'_\mu. \end{aligned} \quad (3)$$

Here, A_n^x and A_n^y are functions of the lattice coordinates n , playing the role of a synthetic magnetic vector potential. These gauge relations generalize the criterion used in Ref. [7], which involved phase differences in the tight-binding hopping amplitudes.

Suppose the vector potential is associated with a uniform rational magnetic flux through each unit cell: $A_n^x + A_{n+x}^y - A_{n+y}^x - A_n^y = 2\pi P/Q$, where P and Q are integers. When $Q = 1$, i.e. for any integer number of flux quanta through each unit cell, we can show that the band structure is the same as in the “zero field” ($A_n^x = A_n^y = 0$) system. In this case, the magnetic unit cell has the same periodicity as the lattice, and the system supports solutions of the form

$$a_{n+\mu} = e^{i(K_\mu + A_n^\mu)} a_n, \quad b_{n+\mu} = e^{i(K_\mu + A_n^\mu)} b_n. \quad (4)$$

Inserting (3) into (1) yields the quadratic equation [23]

$$e^{-4i\phi} - B e^{-2i\phi} - C = 0, \quad (5)$$

where

$$\begin{aligned} B &= r'_x t'_y e^{iK_x} + r_x t_y e^{-iK_x} + t_x r'_y e^{iK_y} + t'_x r_y e^{-iK_y} \\ C &= (r_x r'_x - t_x t'_x)(r_y r'_y - t_y t'_y). \end{aligned}$$

As we shall see, for unitary couplings this gives four real bands in the periodic space $\phi \in [-\pi, \pi]$: two in $[-\pi/2, \pi/2]$ obtained by directly solving (5), and the other two by adding $\pm\pi$. Since the vector potential does not appear in the dispersion relation, the band structure for any integer number of flux quanta per unit cell is the same as for the zero-field system. This property relies crucially on the fact that in (3) there is no phase variation in the $\{t_{n\mu}, t'_{n\mu}\}$ coefficients. For the waveguide coupler shown in Fig. 1(c), this condition is satisfied if the sum of the phase delays on the two arms of the coupler is kept constant [23].

The behavior of the zero-field (or integer flux) system is not as simple as one might initially suppose. The system possesses an inherent degree of non-reciprocity in each spin sector, arising from the coupling equations (1); as it turns out, this gives rise to a topological insulator state (or, within each spin sector, a zero-field quantum Hall effect [3]). The rest of this Letter will focus on this case. As for non-integer fluxes ($Q \neq 1$), the present approach gives essentially the same physics as the tight-binding analysis of Ref. [7]: using the Landau gauge $A_n^x = (P/Q) y_n$ and $A_n^y = 0$, we can define a $Q \times 1$ magnetic unit cell in which the amplitudes obey

$$a_{n+Qx} = e^{i(K_x + Py_n)} a_n, \quad a_{n+y} = e^{iK_y} a_n, \quad (6)$$

and similarly for b . This gives rise to $4Q$ bands, analogous to Landau levels in the two-dimensional magnetized electron gas. The band structure may be obtained by a multi-cell calculation, and a Hofstadter butterfly spectrum is obtained by continuously varying the magnetic flux [7, 13].

If the couplings conserve energy, the coupling matrices are unitary: $S_\mu^\dagger = S_\mu^{-1}$. In this situation, we expect the band structure $\phi(K_x, K_y)$ to be real (for K_x and K_y real). This is easily proven by using the parameterization

$$\begin{aligned} r_\mu &= \sin \theta_\mu e^{i\chi_\mu}, & t'_\mu &= -\cos \theta_\mu e^{i(\varphi_\mu - \xi_\mu)}, \\ t_\mu &= \cos \theta_\mu e^{i\xi_\mu}, & r'_\mu &= \sin \theta_\mu e^{i(\varphi_\mu - \chi_\mu)}, \end{aligned} \quad (7)$$

where $\theta_\mu \in [0, \pi/2]$ and $\chi_\mu, \xi_\mu, \varphi_\mu \in [0, 2\pi]$. For the zero-field system, Eq. (5) then simplifies to

$$e^{-4i\tilde{\phi}} + 2iY e^{-2i\tilde{\phi}} - 1 = 0, \quad (8)$$

where

$$\begin{aligned} Y &\equiv \sin \theta_x \cos \theta_y \sin \tilde{K}_x - \cos \theta_x \sin \theta_y \sin \tilde{K}_y \\ \tilde{\phi} &\equiv \phi + \frac{\varphi_x + \varphi_y}{4} \\ \tilde{K}_x &\equiv K_x + \frac{\varphi_x}{2} - \chi_x + \frac{\varphi_y}{2} - \xi_y \\ \tilde{K}_y &\equiv K_y + \frac{\varphi_y}{2} - \chi_y - \frac{\varphi_x}{2} + \xi_x. \end{aligned} \quad (9)$$

For real K_μ ,

$$|Y| \leq \sin(\theta_x + \theta_y) \leq 1, \quad (10)$$

and hence Eq. (9) yields real bands of the form

$$\begin{aligned} \phi_+ &= m\pi - \frac{\varphi_x + \varphi_y}{4} + \frac{1}{2} \sin^{-1} [Y(K_\mu)] \\ \phi_- &= n\pi - \frac{\varphi_x + \varphi_y}{4} + \frac{1}{2} \{\pi - \sin^{-1} [Y(K_\mu)]\}. \end{aligned} \quad (11)$$

The above calculation also yields the phase diagram. Band-crossing points occur if, and only if, the inequality (10) can saturate, i.e. $\theta_x + \theta_y = \pi/2$, or equivalently $|r_x|^2 + |r_y|^2 = 1$. This defines a boundary between two distinct insulator phases, one of which turns out to be topologically non-trivial. In order to demonstrate this, we specialize to $\varphi_\mu = \chi_\mu = 0$, $\xi_\mu = \pi/2$, and $\theta_x = \theta_y = \theta$, so that S_μ is symmetric ($t_\mu = t'_\mu = i \cos \theta$), and

$$Y = -\frac{1}{2} \sin 2\theta [\cos K_x + \cos K_y]. \quad (12)$$

The projected band diagram for a semi-infinite “lattice strip” (which has a finite width in the y direction and is infinite in the x direction) can be calculated in a similar way [23]. Fig. 2 shows the results for several values of θ . For $\theta < \pi/4$, the band gap contains edge states with both group velocities on each edge, corresponding to a trivial insulator. For $\theta > \pi/4$, the system is a topological insulator: within the given spin sector (clockwise), there is one single positive group velocity mode confined to the upper edge, and one negative group velocity mode confined to the lower edge (Fig. 3).

We note that these results would not show up in the tight-binding analysis of Ref. [7], where tight-binding amplitudes were assigned to the resonator modes. The

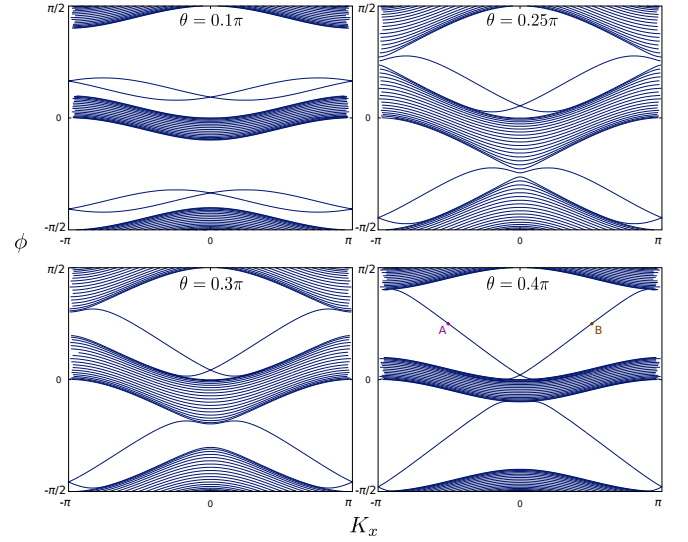


FIG. 2. Projected band diagram for the semi-infinite resonator lattice, with 20 lattice sites in the y direction. The coupling coefficients are given by Eq. (7) with $\varphi_\mu = \chi_\mu = 0$, $\xi_\mu = \pi/2$, and $\theta_x = \theta_y = \theta$. The synthetic gauge field defined in Eq. (3) is zero. The bands are degenerate when $\theta = \pi/4$ (upper right-hand figure). For $\theta > \pi/4$, each band gap is populated by a pair of one-way edge states. In the $\theta = 0.4\pi$ plot, the points labeled A and B , located at $\phi = \pi/4$, indicate the edge states whose intensity profiles are shown in Fig. 3.

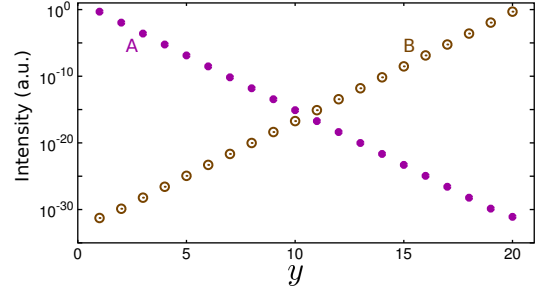


FIG. 3. Variation of edge state intensity with y lattice coordinate, demonstrating single-edge confinement and exponential decay into the bulk. The two edge states, labeled A (filled circles) and B (open circles), have equal $\phi = \pi/4$, and occur at $K_x = \mp 1.587$ respectively, with opposite group velocities. The lattice parameters are those used in Fig. 2, with $\theta = 0.4\pi$. We are considering the clockwise spin sector, as depicted in Fig. 1. The intensities are defined as the mean of the squared wave amplitudes on the four arms of the resonator at each lattice site, i.e. $(|a_n|^2 + |b_n|^2 + |c_n|^2 + |d_n|^2)/4$.

topological insulator phase, $\theta_x + \theta_y > \pi/2$, corresponds to strong coupling between the resonators, rather than weak coupling. Furthermore, the one-way edge states arise from the internal structure of the modes at each lattice site. Intuitively, each edge state corresponds to a mode which undergoes critical coupling from resonator to resonator along one edge, which only occurs if the propagation direction along that edge coincides with the

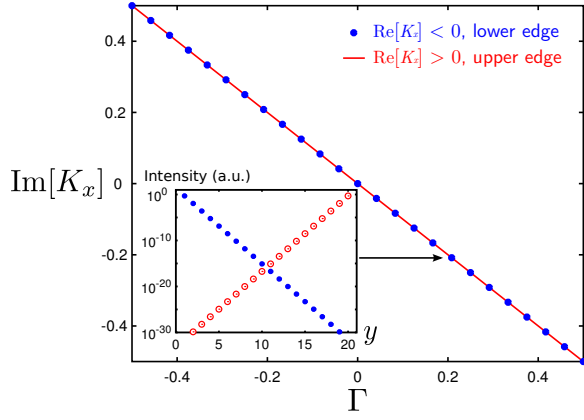


FIG. 4. Amplification and damping of the edge states induced by the PT symmetric gain/loss parameter Γ , defined in Eq. (15). All other coupling parameters are the same as in Fig. 2, with $\theta = 0.4\pi$. Both edge states acquire an imaginary component $-i\Gamma$ to the wave vector, resulting in one edge state being damped and the other amplified. Inset: the intensity profiles of the two edge states at $\Gamma = 0.2$, showing that they remain well-confined.

chosen direction of rotation within each resonator.

Finally, we study what happens when the resonator lattice is PT-symmetric. PT-symmetric topological insulators are probably impossible to realize in condensed-matter systems, but may be possible in optical resonator systems, where gain and loss can be selectively added to the resonators and/or coupling waveguides. The transfer matrix method is well-suited for studying this: we simply replace the unitary coupling matrices with matrices obeying the PT-symmetry relation for scattering matrices [24–26]:

$$\mathcal{PT} S_\mu \mathcal{PT} = S_\mu^{-1}. \quad (13)$$

Here, \mathcal{P} is a parity operator and \mathcal{T} is a time-reversal operator. We choose $\mathcal{P} = [0, 1; 1, 0]$ and \mathcal{T} to be the complex conjugation operator. For the setup shown in Fig. 1(c), setting $\psi_2 = \psi_1^*$ causes S_μ to satisfy (13) with this representation of \mathcal{P} and \mathcal{T} . The coupling coefficients can in general be parameterized by

$$\begin{aligned} r &= |r| e^{i\varphi}, & t' &= -|t| e^{i(\varphi - \varphi')}, \\ t &= |t| e^{i(\varphi + \varphi')}, & r' &= |r'| e^{i\varphi}, \end{aligned} \quad (14)$$

with $|rr'| + |t|^2 = 1$. Note that this parameterization differs slightly from that of Ref. [26], which considers reciprocal systems, for which the scattering matrices are symmetric; our S_μ 's need not be symmetric. For convenience, however, we set $\varphi = 0$ and $\varphi' = \pi/2$. The coefficients then have the form

$$\begin{aligned} r &= e^\Gamma \sin \theta, & t' &= i \cos \theta, \\ t &= i \cos \theta, & r' &= e^{-\Gamma} \sin \theta. \end{aligned} \quad (15)$$

The gain/loss parameter Γ characterizes the strength of the unitarity breaking, with $\Gamma = 0$ corresponding to the unitary coupling considered previously.

Fig. 4 shows the effect of PT-symmetric gain/loss on the edge states of the semi-infinite strip. Here, we introduce non-zero Γ to the couplings in the x direction, while keeping the y couplings unitary [27]. The two edge states (which are localized to opposite edges and have opposite group velocities) acquire the same imaginary component to their wave vectors. Thus, one of them is damped and the other amplified. This has a simple interpretation in terms of the coupling scheme shown in Fig. 1(c): if we add gain to (say) the lower arm of the coupling waveguide and loss to the upper arm, the backward-propagating edge state (on the lower edge) is concentrated in the upper coupler arms, and is damped; while the forward-propagating edge state (on the upper edge) is concentrated in the lower coupler arms, and is amplified. Previous authors have studied PT-symmetric waveguides, and demonstrated that modes concentrated at different transverse positions can be selectively amplified and damped [20]. Such waveguides, however, are reciprocal, so each amplified (damped) mode has a counter-propagating partner which is amplified (damped) by an equal amount. In the present system, topological insulator edge states have no counter-propagating partners in the same spin sector. Hence, if we consider the entire strip (rather than a single edge) as an optical waveguide, the introduction of PT-symmetric gain/loss gives us a directional amplifier, or optical diode. Furthermore, unlike the PT-symmetric diode studied in Ref. [28], this device does not require optical nonlinearity.

This research was supported by the Singapore National Research Foundation under grant No. NRFF2012-02. We are grateful to J. M. Taylor for helpful discussions.

Supplementary material

Appendix A: Inter-loop Coupling Coefficients

In Eq. (1), we abstract away the couplings between resonators into a set of “reflection coefficients” and “transmission coefficients”, reproduced here for convenience:

$$S_{nx} \begin{bmatrix} a_n \\ b_{n+x} \end{bmatrix} = \begin{bmatrix} d_{n+x} \\ c_n \end{bmatrix}, \quad (\text{A1})$$

$$S_{ny} \begin{bmatrix} d_n \\ c_{n+y} \end{bmatrix} = \begin{bmatrix} b_{n+y} \\ a_n \end{bmatrix} e^{-2i\phi}, \quad (\text{A2})$$

$$S_{n\mu} = \begin{bmatrix} r_{n\mu} & t'_{n\mu} \\ t_{n\mu} & r'_{n\mu} \end{bmatrix}. \quad (\text{A3})$$

In this section, we discuss how these coefficients can be related to the parameters of the underlying waveguide-coupling mechanism, such as that discussed in Ref. [7]. As shown in Fig. 1(c), the resonator amplitudes a , b , c , and d (we will omit the redundant subscripts for simplicity) are coupled to waveguide amplitudes α , β , γ , and δ , by coupling relations [16]:

$$\begin{bmatrix} \tau & i\kappa \\ i\kappa & \tau \end{bmatrix} \begin{bmatrix} a \\ \alpha \end{bmatrix} = \begin{bmatrix} c \\ \gamma \end{bmatrix} \quad (\text{A4})$$

$$\begin{bmatrix} \tau' & i\kappa' \\ i\kappa' & \tau' \end{bmatrix} \begin{bmatrix} b \\ \beta \end{bmatrix} = \begin{bmatrix} d \\ \delta \end{bmatrix}. \quad (\text{A5})$$

Without loss of generality, τ , τ' , κ , and κ' may be taken to be real. If the phase delays along the two arms of the waveguide are ψ_1 and ψ_2 respectively, then

$$\alpha = e^{i\psi_2} \delta, \quad \beta = e^{i\psi_1} \gamma. \quad (\text{A6})$$

By combining Eqs. (A4)-(A6), we obtain

$$\begin{bmatrix} d \\ c \end{bmatrix} = \frac{1}{1 - \tau\tau'e^{i(\psi_1+\psi_2)}} \begin{bmatrix} -\kappa\kappa'e^{i\psi_1} & \tau' - \tau e^{i(\psi_1+\psi_2)} \\ \tau - \tau' e^{i(\psi_1+\psi_2)} & -\kappa\kappa'e^{i\psi_2} \end{bmatrix} \begin{bmatrix} a \\ b \end{bmatrix}. \quad (\text{A7})$$

Comparison with (A1)-(A3) immediately yields the corresponding values of r , r' , t , and t' .

As indicated in Ref. [7], the synthetic magnetic vector potential can be implemented by altering the phase delay ψ_1 on different lattice points, while keeping $\psi_1 + \psi_2$ fixed. This leaves the t and t' coefficients, which are given by the off-diagonal matrix elements in (A7), independent of ψ_1 , in agreement with Eq. (3). The relevant component of the resulting vector potential is $A = \psi_1$.

Appendix B: Gauge Transformations

In this section, we provide additional details about the gauge structure of the resonator lattice. The coupling relations between resonator amplitudes, given by (A1)-(A3), can be simplified by eliminating the c and d variables, which yields

$$\begin{aligned} e^{-2i\phi} b_n - r_{n-y,y} t'_{n-x-y,x} b_{n-y} - t'_{n-y,y} r'_{n,x} b_{n+x} &= r_{n-y,y} r_{n-x-y,x} a_{n-x-y} + t'_{n-y,y} t_{n,x} a_n \\ e^{-2i\phi} a_n - t_{n,y} r_{n-x,x} a_{n-x} - r'_{n,y} t_{n+y,x} a_{n+y} &= r'_{n,x} r'_{n+y,x} b_{n+x+y} + t_{n,y} t'_{n-x,x} b_n. \end{aligned} \quad (\text{B1})$$

When the coupling coefficients obey the gauge relations (3), the system of equations (B1) simplifies to

$$\begin{aligned} e^{-2i\phi} b_n - t'_x r_y e^{iA_{n-y}^y} b_{n-y} - r'_x t'_y e^{-iA_n^x} b_{n+x} &= r_x r_y e^{i(A_{n-x-y}^x + A_{n-y}^y)} a_{n-x-y} + t_x t'_y a_n \\ e^{-2i\phi} a_n - r_x t_y e^{iA_{n-x}^x} a_{n-x} - t_x r'_y e^{-iA_n^y} a_{n+y} &= r'_x r'_y e^{-i(A_{n+y}^x + A_n^y)} b_{n+x+y} + t'_x t_y b_n. \end{aligned} \quad (\text{B2})$$

We look for solutions to these two equations, using the Bloch ansatz (4). When writing down the amplitudes for negative displacements and/or composed displacements using this ansatz, some care is needed to ensure that the A 's are evaluated at lattice positions consistent with (4). For example,

$$\begin{aligned} a_{n-x} &= e^{-i(K_x + A_{n-x}^x)} a_n \\ a_{n+x+y} &= e^{i(K_x + K_y + A_{n+y}^x + A_n^y)} a_{n+y} \\ a_{n-x-y} &= e^{-i(K_x + K_y + A_{n-x-y}^x + A_{n-y}^y)} a_n, \text{ etc.} \end{aligned} \quad (\text{B3})$$

Plugging these relations into (B2) yields

$$\begin{aligned} \left[e^{-2i\phi} - r'_x t'_y e^{iK_x} - t'_x r_y e^{-iK_y} \right] b_n &= \left[r_x r_y e^{-i(K_x + K_y)} + t_x t'_y \right] a_n \\ \left[e^{-2i\phi} - r_x t_y e^{-iK_x} - t_x r'_y e^{iK_y} \right] a_n &= \left[r'_x r'_y e^{i(K_x + K_y)} + t'_x t_y \right] b_n. \end{aligned} \quad (\text{B4})$$

The resulting dispersion relation (ϕ versus K_x and K_y) is independent of A_n^x and A_n^y .

Appendix C: Projected band diagram

The calculation of the projected band diagram for the resonator lattice is much like the calculation of the CROW's dispersion relation by Yariv *et al.* [16]. Suppose we have a semi-infinite strip, whose width is N lattice sites in the y direction and infinite in the x direction, with the coupling matrices independent of the x coordinate. We seek solutions of the form

$$[a, b, c, d]_{n+x} = e^{iK_x} [a, b, c, d]_n.$$

Let us consider a single column of the lattice, and replace the site index n with $j \in \{1, 2, \dots, N\}$ denoting the y coordinate. From (A1),

$$M_j^x \begin{bmatrix} c_j \\ a_j \end{bmatrix} = e^{iK_x} \begin{bmatrix} b_j \\ d_j \end{bmatrix} \quad \text{where} \quad M_j^x \equiv \frac{1}{r'_{jx}} \begin{bmatrix} 1 & -t_{jx} \\ t'_{jx} & \det[S_{jx}] \end{bmatrix}. \quad (\text{C1})$$

From (A2),

$$M_j^y(\phi) \begin{bmatrix} d_j \\ b_{j+1} \end{bmatrix} = \begin{bmatrix} a_j \\ c_{j+1} \end{bmatrix} \quad \text{where} \quad M_j^y(\phi) \equiv \frac{1}{t'_{jy}} \begin{bmatrix} -e^{2i\phi} \det[S_{jy}] & r'_{jy} \\ -r_{jy} & e^{-2i\phi} \end{bmatrix}, \quad (\text{C2})$$

for $j = 1, \dots, N-1$. At the edges of the lattice, we have the boundary conditions (refer to Fig. 1 of the paper):

$$c_1 = e^{-2i\phi} b_1, \quad a_N = e^{2i\phi} d_N. \quad (\text{C3})$$

Combining (C1)-(C3) yields the eigenvalue equation

$$M_A M_B \begin{bmatrix} b_1 \\ d_1 \\ \vdots \\ b_N \\ d_N \end{bmatrix} = e^{iK_x} \begin{bmatrix} b_1 \\ d_1 \\ \vdots \\ b_N \\ d_N \end{bmatrix}, \quad (\text{C4})$$

where M_A and M_B are the following $2N \times 2N$ matrices:

$$M_A = \begin{bmatrix} M_1^x & & & \\ & M_2^x & & \\ & & \ddots & \\ & & & M_N^x \end{bmatrix}, \quad M_B = \begin{bmatrix} e^{-2i\phi} & & & \\ & M_1^y & & \\ & & \ddots & \\ & & & M_{N-1}^y \\ & & & & e^{2i\phi} \end{bmatrix}. \quad (\text{C5})$$

To generate the projected band diagram, we sweep ϕ through the desired range (usually $[-\pi/2, \pi/2]$ due to the π -periodicity of the band structure), solving the eigenvalue problem (C4) at each ϕ . The eigenvalues which do not have

unit modulus, which correspond to evanescent modes, are discarded; the arguments of the rest are the value(s) of K_x for that value of ϕ .

-
- [1] F. D. M. Haldane and S. Raghu, Phys. Rev. Lett. **100**, 013904 (2008).
 - [2] S. Raghu and F. D. M. Haldane, Phys. Rev. A **78**, 033834 (2008).
 - [3] F. D. M. Haldane, Phys. Rev. Lett. **61**, 2015 (1988).
 - [4] Z. Wang, Y. D. Chong, J. D. Joannopoulos, and M. Soljačić, Phys. Rev. Lett. **100**, 013905 (2008).
 - [5] Z. Wang, Y. D. Chong, J. D. Joannopoulos, and M. Soljačić, Nature **461**, 772 (2009).
 - [6] J. Koch, A. A. Houck, K. L. Hur, and S. M. Girvin, Phys. Rev. A **82**, 043811 (2010).
 - [7] M. Hafezi, E. A. Demler, M. D. Lukin, and J. M. Taylor, Nature Physics **7**, 907 (2011).
 - [8] T. Ochiai, Phys. Rev. B **86**, 075152 (2012).
 - [9] K. Fang, Z. Yu, and S. Fan, Nature Photonics **6**, 782 (2012).
 - [10] V. Yannopapas, N. J. Phys. **14**, 113017 (2012).
 - [11] A. B. Khanikaev, S. H. Mousavi, W.-K. Tse, M. Kargarian, A. H. MacDonald, and G. Shvets, arXiv:1204.5700.
 - [12] A. Yariv, Y. Xu, R. K. Lee, and A. Scherer, Opt. Lett. **24**, 711 (1999).
 - [13] D. R. Hofstadter, Phys. Rev. B **14**, 2239 (1976).
 - [14] C. L. Kane and E. J. Mele, Phys. Rev. Lett. **95**, 226801 (2005).
 - [15] A. Yariv, IEEE Phot. Tech. Lett. **14**, 483 (2002).
 - [16] J. K. S. Poon, J. Scheuer, S. Mookherjee, G. T. Paloczi, Y. Huang, and A. Yariv, Opt. Ex. **12**, 90 (2004).
 - [17] C. M. Bender and S. Boettcher, Phys. Rev. Lett. **80**, 5243 (1998).
 - [18] K. G. Makris et al., Phys. Rev. Lett. **100**, 103904 (2008); Phys. Rev. A **81**, 063807 (2010).
 - [19] Z. H. Musslimani, K. G. Makris, R. El-Ganainy, and D. N. Christodoulides, Phys. Rev. Lett. **100**, 030402 (2008); J. Phys. **A** **41**, 244019 (2008).
 - [20] A. Guo et al., Phys. Rev. Lett. **103**, 093902 (2009).
 - [21] C. E. Ruter et al., Nature Phys. **6**, 192 (2010).
 - [22] A. Regensburger, C. Bersch, M.-A. Miri, G. Onishchukov, D. N. Christodoulides, and U. Peschel, Nature **488**, 167 (2012).
 - [23] See Supplementary Material.
 - [24] H. Schomerus, Phys. Rev. Lett. **104**, 233601 (2010).
 - [25] Y. D. Chong, L. Ge, and A. D. Stone, Phys. Rev. Lett. **106**, 093902 (2011).
 - [26] L. Ge, Y. D. Chong and A. D. Stone, Phys. Rev. A **85**, 023802 (2012).
 - [27] Adding gain/loss to the y couplings, while keeping the x couplings unitary, causes the projected band structure to remain strictly real (including the edge states).
 - [28] H. Ramezani, T. Kottos, R. El-Ganainy, and D. N. Christodoulides, Phys. Rev. A **82**, 043803 (2010).